## SEMICONDUCTOR/ELECTROLYTE BOUNDARIES

Since the development of the first integrated circuit in 1958, progress in fabrication techniques has resulted in continued improvements in miniaturization and computing power. Planar integrated circuit technology is based largely on silicon. Other important semiconductors are III-V compound materials such as GaAs, InP, GaP and the many ternary compound materials which are used in optoelectronic devices such as light emitting diodes (*LED*'s), optical detectors, and lasers. In addition, many II-VI materials including the oxide semiconductors ZnO and $TiO_2$, as well as sulfides and selenides such as CdS, ZnSe, have been shown to exhibit unique electrical and optical properties. The properties of a wide range of materials ranging from passive films on metals to organic materials such as conducting polymers have also been analyzed and explained on the basis of semiconductor physics.

High quality wafers of materials such as silicon are usually produced from the melt. Large boules of the crystal are subsequently sliced into thin wafers which are used as the starting point in the fabrication of electronic devices. With current processing techniques, the quality of the bulk material is very good and the limiting factor determining the yield of working devices is often related to the surface characteristics of the semiconductor wafer. As a consequence, much research has been focused on the surface properties and the semiconductor/electrolyte boundary has become of great interest, not only from a fundamental point of view but also for the advance of semiconductor technology (1).

In this paper, we describe the fundamental principles governing the electrical properties of semiconductor/electrolyte boundaries. In the first section, the energetics of semiconducting materials are described including the energy band structure, *n*-type and *p*-type doping, and the concept of the Fermi energy. In the second section, the structure of the electrical double layers at the semiconductor/electrolyte interface is treated in detail, and the consequences of the energy band structure for the electrical processes at the interface are explained. The third section describes the influence of interfacial layers, electrically active surface states, and recombination centers at the surface. Various modulation techniques which can be used to elucidate the kinetics of surface-related processes are described. The main focus is on electrochemical impedance spectroscopy both in the dark and under illumination, as well as intensity modulated photocurrent spectroscopy and potential modulated microwave reflectivity spectroscopy. Examples of recent results on silicon are given to illustrate the application of these three methods.

### ENERGY BAND STRUCTURE

Crystalline materials form a network of covalent or ionic bonds which gives rise to a well-defined energy band structure. This can be understood from molecular orbital theory which describes the splitting of discrete atomic orbitals into bonding and anti-bonding orbitals upon interaction with other atoms. The energy levels of identical overlapping atomic orbitals cannot be equal and, as a result, a large number of closely spaced energy levels are created in the macroscopic solid which can be regarded as energy bands. These energy bands can be several electron volts wide. The electrical conductivity of the solid and its electrochemical characteristics are mainly determined by the highest occupied and the lowest empty energy band denoted the valence band and the conduction band, respectively. The valence band usually corresponds to bonding orbitals and contains the bonding electrons. The conduction band generally corresponds to anti-bonding orbitals and is usually empty. The valence and conduction bands may be separated by a characteristic energy gap, which is a key parameter in determining the physical properties of the material, including electrical and optical properties, such as conductivity and photoconductivity. For a more detailed description of the band structure of materials, the reader is referred to References (2, 3).

Electrical conductivity arises when charge carriers can move through the crystal under the influence of a concentration gradient or an electric field. In metals, the valence or conduction bands are either only partially filled, or the valence band and the conduction band overlap. As a consequence, only very little additional energy is needed to promote electrons to empty energy levels, leading to a large electrical conductivity. Insulators are characterized by a large energy band gap ($E_g > 3$ eV) between the completely filled valence and empty conduction bands, and a low density of mobile charge carriers. As a result, the electrical conductivity of the material is small. Semiconductors generally have an energy band gap between about 0.1 eV and 3 eV and are characterized by a conductivity between that of metals and insulators. In addition, insulators can be made semiconducting by doping the material with electron donating or accepting impurities; this doping process is described in more detail in a later section.

In semiconductors two types of charge carrier are present: negatively charged electrons in the conduction band (*CB*) and positively charged "holes" in the valence band (*VB*). A hole in the valence band corresponds to the absence of a bonding electron; motion of a hole can be seen as consecutive jumps of bonding electrons from their site in the crystal to the empty site, i.e., the hole. Both types of charge carrier are delocalized over the entire crystal and are, therefore, free carriers. Within the conduction band, an electron will assume the energy of the lowest unoccupied level, while a free hole will be at the energy of the highest filled level in the valence band. As a consequence, the energetic position of the conduction and valence band edges are important parameters for electrical processes.

In an intrinsic semiconductor devoid of defects or impurities, free charge carriers can only be formed by exciting an electron from the valence band to the conduction band. Consequently, the density of holes (VB) and electrons (CB) are equal. In this case, the energy gap between the bands determines the conductivity of the material: if the energy gap is small ($E_g < 0.5$ eV), the conductivity at room temperature can be fairly large as thermal vibrations are sufficient to excite electrons from the valence band to the

conduction band, while for larger energy gaps the conductivity at room temperature is small. The conductivity of intrinsic semiconductors can be enhanced greatly by irradiating the material with light of a wavelength sufficiently small to promote electrons from the valence band to the conduction band. This principle is the basis of the photosensitivity of semiconductors, which is extensively used in practical devices such as solar cells and optical detectors (4).

In general, however, crystals are not perfect and contain impurities which greatly affect the electrical properties of the material. Impurities may be intentionally introduced in order to change the electrical conductivity, or may be a result of the crystal growing method. The electrical properties of the material are dependent on the dopant type, concentration, and distribution. The effect of doping on the electrical conductivity is easily illustrated using silicon as an example. Silicon is a Group IVA element with four valence electrons involved in the chemical bonding structure. Good quality intrinsic silicon has a conductivity of about $10^{-4}$ S cm$^{-1}$ at room temperature; for comparison, the conductivity of copper at room temperature is about $10^{6}$ S cm$^{-1}$. If a Group VA element with five bonding electrons, such as phosphorus, is incorporated into the silicon crystal, one electron cannot participate in the lattice bonding and is localized at a relatively high energy, spatially close to the phosphorus atom. For the case of phosphorus, the energy of this extra electron is close to the edge of the conduction band and thermal energy is sufficient to free the electron from the phosphorus atom and the electron becomes delocalized in the conduction band. Phosphorus is called a donor and since no free holes (VB) are created, only electrons (CB) carry the current and the silicon is doped "*n*-type". In this case, electrons (CB) are called the majority carriers and holes (VB) the minority carriers. The conductivity is mainly dependent on the density of built-in phosphorus atoms: the conductivity can be adjusted between $10^{-4}$ S cm$^{-1}$ and $10^{4}$ S cm$^{-1}$ for doping levels of $10^{12}$ cm$^{-3}$ to about $10^{21}$ cm$^{-3}$; the number of silicon atoms is $5 \times 10^{22}$ cm$^{-3}$. If, on the other hand, a Group IIIA element such as boron is incorporated into the lattice, one additional electron is required for the bonds, which creates an energy level just above the valence band edge. An electron from the valence band may be thermally excited to this level which creates a free, delocalized hole in the valence band; boron is an electron acceptor. In this case, holes (VB) are the majority carriers. The silicon is *p*-type and the conductivity can be similarly adjusted. The doping process is also applicable to high band gap materials such as many metal oxides and diamond, which are insulators in the intrinsic form.

These concepts are illustrated in Figure 1. Figure 1a shows the energy band structure of an intrinsic semiconductor; one electron (CB) and one hole (VB) are included which may have been created thermally or by absorption of a photon of energy larger than the energy band gap. Figures 1b and 1c show the energy band structure of *n*-type and *p*-type semiconductors. Note that the electron donating and accepting atoms are spatially localized; at room temperature the donor levels will be empty and positively charged, while the acceptor levels are filled and hold a negative charge.

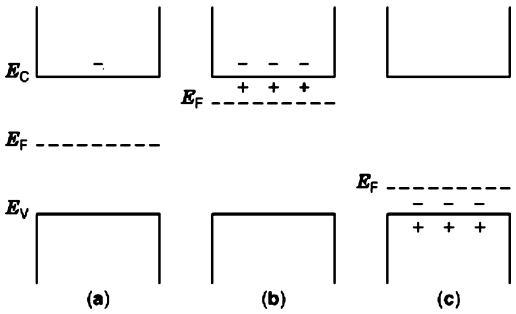


**Figure 1.** Energy band diagrams for (a) intrinsic, (b) *n*-type doped, and (c) *p*-type doped semiconductors. $E_C$ and $E_V$ represent the lowest unoccupied and highest occupied levels in the conduction band and valence band, respectively. The holes in the valence band and electrons in the conduction band are delocalized over the crystal, while the ionized donors and acceptors are spatially localized.

The Fermi energy is an important concept in semiconductor electrochemistry since it is a parameter that can be controlled by an externally applied potential. Thermodynamically, the Fermi energy corresponds to the electrochemical potential of electrons in the material ($\overline{\mu}_e$). The probability that an energy level at the Fermi energy is occupied is exactly 0.5; the occupancy probability of levels is described by the Fermi–Dirac distribution:

$$f(E) = \frac{1}{1 + \exp[(E - E_F)/k_B T]} \tag{1}$$

where $f(E)$ is the probability that a level at energy $E$ is occupied, $E_F$ is the Fermi energy, $k_B$ is the Boltzmann constant, and $T$ is the absolute temperature. Equation (1) shows that the probability of occupancy of energy levels at energies more than $3kT$ below the Fermi energy is almost 1, while energy levels above the Fermi energy are most likely empty. For intrinsic semiconductors the Fermi energy is close to the middle of the energy band gap. If the semiconductor is doped, the Fermi energy shifts due to the presence of the free carriers occupying energy levels in the conduction or valence band: for *n*-type doping the Fermi energy shifts up towards the conduction band edge while for *p*-type doping the shift is in the direction of the valence band edge. The energy difference between the Fermi energy and the two bands depends on the dopant density and is given by Eqs. (2a) and (3b) for *n*-type and *p*-type materials, respectively:

$$E_C - E_F = k_B T \ln\left(\frac{N_C}{N_D}\right) \tag{2a}$$

$$E_F - E_V = k_B T \ln\left(\frac{N_V}{N_A}\right) \tag{2b}$$

where $E_C$ and $E_V$ are the energies of the conduction and valence band edge, $N_C$ and $N_V$ are the effective densities of energy levels in the conduction and valence band, $N_D$ and $N_A$ are the densities of the donor and acceptor atoms, respectively. Figure 1 illustrates the influence of doping on the Fermi energy.

The energy band structure determines many properties of a semiconductor. However, the surface of a semiconductor crystal is inherently different from the bulk and it is important to realize that many specific surface effects may arise which are difficult to explain with the energy band model described above. In ultra high vacuum conditions, the surface atoms of an ideal (111) oriented silicon surface have three instead of four neighboring atoms, hence, a localized bonding orbital with one valence electron is not involved in the bonding structure. This is called a "dangling bond" and the associated energy levels may be quite different from the bulk levels. These surface states can act as donor levels or acceptor levels, and they may form a two-dimensional reconstruction so that the crystal structure of the surface is different from that of the bulk. For crystals with a more ionic character such as ZnO, the termination of the periodicity of the charge density at the surface may also give rise to surface states. In a solution, the dangling bonds are expected to react with species in the solution to form new surface bonds. The energy levels associated with surface states may be in the energy band gap and they may have a distinct influence on the electrical properties of the semiconductor (5–7).

## SEMICONDUCTOR/SOLUTION INTERFACE

When a semiconductor is introduced into a solution, thermodynamic equilibrium is attained when the electrochemical potential of the electrons in the two phases are equal. The electrochemical potential of the solution is generally associated with the energy of a redox couple (for instance, $Fe^{3+}/Fe^{2+}$). The energy levels corresponding to the reduced species (e.g., $Fe^{2+}$) can be interpreted as the occupied levels, and the levels of the oxidized species (e.g., $Fe^{3+}$) as the empty levels. Hence, the "Fermi energy" of the solution is generally taken to be the equilibrium potential of the redox couple, defined by the Nernst equation. In order to attain equilibrium in the system, the Fermi energy of the semiconductor should become equal to that of the solution and charge transfer will occur across the interface until this situation is reached. As a consequence, the interface is characterized by regions with a net charge and an associated potential drop. This process is illustrated schematically in Figure 2 for an *n*-type semiconductor. Typically, electrons are transferred from the *n*-type semiconductor to the electrolyte in order to attain equilibrium and, as a result, a surface layer of the semiconductor becomes depleted of free electrons. As the free electrons are removed from the surface layer, the uncompensated positively charged donor atoms give rise to a positively charged layer at the surface of the semiconductor. The width of this space charge layer depends on the characteristics of the semiconductor (i.e., doping density and dielectric constant) and the initial Fermi energy difference of the two phases. The space charge layer gives rise to a potential drop in the semiconductor between the surface and the bulk; the potential depends quadratically on the distance from the surface which is represented by the band bending shown in Figure 2. The band bending illustrates that the free electron density at the surface is low, as the Fermi energy is lowered further

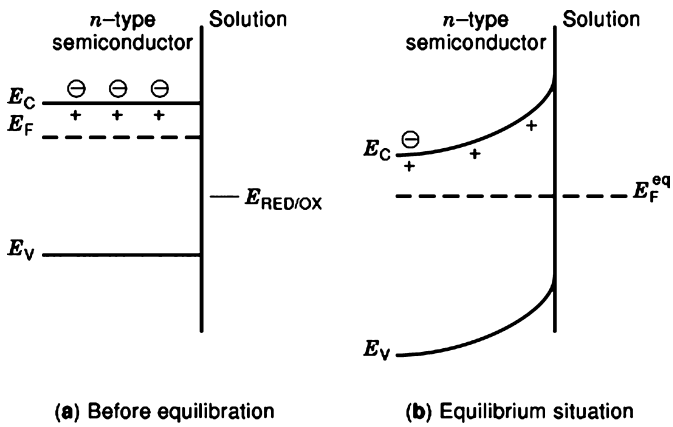


**Figure 2.** Before equilibration (a), the Fermi energies of a semiconductor and an electrolyte solution are different. In the equilibrated situation (b), the Fermi energy is equal in both phases, and a space charge region due to immobile ionized donors has developed at the semiconductor surface. Electrons in the conduction band are depleted from the surface.

below the conduction band edge at the surface (see equation (1)).

On the solution side of the interface a similar process takes place; negative ions are electrostatically attracted to the surface to compensate for the positive charge in the semiconductor. Consequently, a potential drop is generated between the semiconductor surface and the plane of closest approach of the ions in solution, which is called the outer Helmholtz plane. In general, the concentration of ions in the solution should be larger than about 0.1 M to assure that the charge of the semiconductor can be fully compensated by ions at the outer Helmholtz plane. For a more detailed description of the electrostatics in the solution phase see Reference (8). The most important difference between metal and semiconductor electrified interfaces is the width of the space charge layer in the solid: for metals, the conductivity is so large that a depletion layer in the solid does not exist, while in semiconductors the space charge layer is generally much wider than the thickness of the Helmholtz layer. Reviews of semiconductor electrochemistry can be found in References (9–11).

### Impedance of Semiconductor/Electrolyte Solution Interfaces

The charge distribution and the corresponding potential drops across the semiconductor/electrolyte solution interface can be treated quantitatively. As can be inferred from Figure 2, both the space charge layer in the semiconductor and the Helmholtz layer in the solution are characterized by capacitive behavior. In this section, we will derive expressions for the space charge layer capacitance, the Helmholtz layer capacitance, and discuss the influence of adsorption of charged molecules at the surface for the case where water is the solvent.

**Space Charge Layer Impedance.** Figure 3a shows the charge density as a function of distance from the surface, $\rho(x)$, for the situation where electrons are depleted from the surface, assuming that the dopant density is constant

throughout the semiconductor crystal. In the semiconductor, the charge density is constant over a relatively large width while further away from the surface the density decreases to zero since in the bulk all ionized donors are compensated by electrons (CB). In the Helmholtz layer, the charge on the surface is compensated by charge in the plane of closest approach of ions in solution and the opposing charges are separated by a thin layer of polarized solvent molecules. Note that this is only a schematic picture of the interface as the effects of specific adsorption, charged interfacial defects, or the polarization of the first layer of solvent molecules have not been taken into account. In the analysis, a high inert electrolyte concentration is assumed.

The potential distribution in the semiconductor space charge layer will first be calculated, starting from the Poisson equation:

$$\frac{d^2\phi_{sc}}{dx^2} = \frac{-\rho(x)}{\epsilon_r \epsilon_0} \tag{3}$$

where $\phi_{sc}$ is the electrostatic potential which is a function of the distance, x, to the surface, $\varepsilon_r$ is the dielectric constant of the material, and $\varepsilon_0$ is the permittivity of free space. The total charge density contains contributions of ionized donors or acceptors, free electrons, and free holes. For an $n$-type semiconductor (in the absence of illumination), the acceptor density and the density of free holes are negligibly small and $\rho$(x) is given by

$$\rho(x) = e[N_D - n(x)] \tag{4}$$

where $n(x)$ is the density of free electrons as a function of the distance from the surface. The electrons (CB) are in equilibrium throughout the crystal and the Boltzmann equation can be used to describe $n(x)$:

$$n(x) = N_D \exp\left(\frac{e\phi_{sc}}{k_B T}\right) \tag{5}$$

Assuming complete ionization of the donors so that the density of free electrons in the bulk is equal to the density of donors, combining equations (3) to (5) leads to:

$$\frac{d^2\phi_{sc}}{dx^2} = \frac{-eN_D}{\epsilon_r \epsilon_0}\left[1 - \exp\left(\frac{e\phi_{sc}}{k_B T}\right)\right] \tag{6}$$

At the surface ($x$ = 0), the potential is equal to $\phi_s$, and the band bending $\Delta\phi_{sc}$ is defined as ($\phi_b - \phi_s$), where the potential in the bulk, is $\phi_b$ = 0. Integration gives an expression for the electric field at the surface:

$$\left(\frac{d\phi_{sc}}{dx}\right)_{x=0} = \pm\left(\frac{2k_B T N_D}{\epsilon_r \epsilon_0}\right)^{1/2}\left[\exp\left(\frac{e\Delta\phi_{sc}}{k_B T}\right) - \frac{e\Delta\phi_{sc}}{k_B T} - 1\right]^{1/2} \tag{7}$$

where the negative sign is applied when the density of electrons at the surface is larger than in the bulk and $\Delta\phi_{sc} > 0$ (accumulation), and the positive sign holds in the situation where electrons are depleted from the surface ($\Delta\phi_{sc} < 0$) which is shown in Figure 3. Under depletion conditions, the electric field decreases linearly with the distance from the surface as illustrated in Figure 3b. The potential in the space charge layer is obtained by integration of the dependence of the field on the distance, hence, it is found that the potential varies quadratically with distance in the space charge layer which is shown in Figure 3c. As a consequence, the bending of the conduction and valence bands shown in Figure 2 also follow a quadratic dependence on $x$.

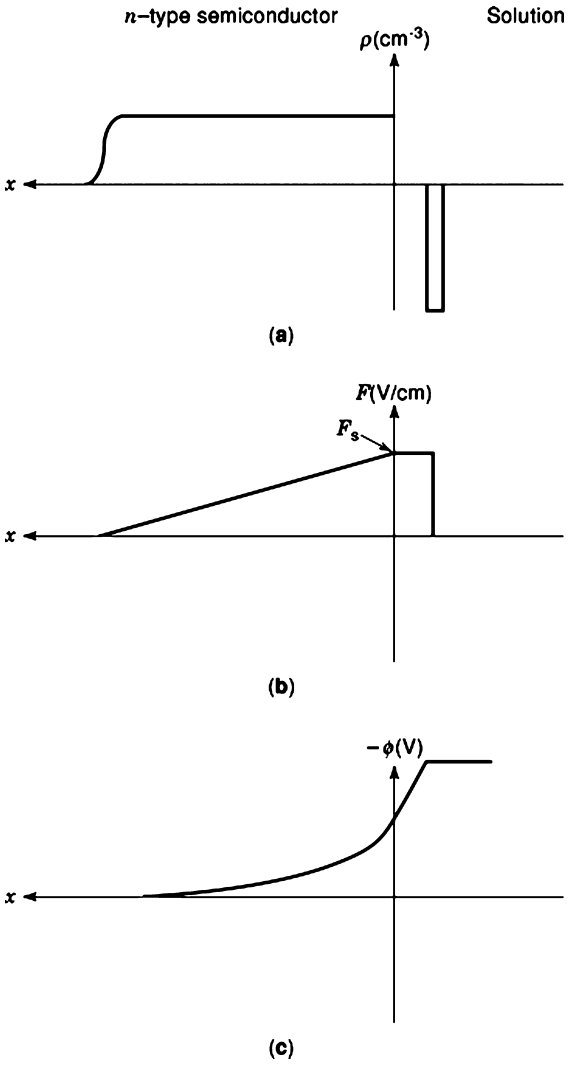


**Figure 3.** The charge (a), the electric field (b), and the electrostatic potential (c) versus distance from the interface for an $n$-type semiconductor in solution for the situation where electrons (CB) are depleted from the surface. Note that the space charge region in the semiconductor is typically a factor 100 or more wider than that in the solution, and that the plots are not to scale. The positive charge in the semiconductor is due to ionized donors, and the counter charge in the solution is separated from the surface by a thin solution layer. The electric field, $F$, calculated from the Poisson equation is shown in (b) (note that this plot is also not to scale). Figure (c) shows the corresponding potential, $\phi$, as a function of the distance from the surface illustrating the quadratic dependence of the band bending in the semiconductor. The curves at the solution side of the interface in (a), (b), and (c) show the ideal situation where the charge trapped at the interface due to surface states, or specific adsorption is neglected: in general, the potential is discontinuous at the interface, and is drawn to be higher on the solution side (see Ref. (9)).

The charge in the space charge layer, $Q_{sc}$, can be related to the field at the surface using Gauss' law, $Q_{sc} = \varepsilon_r \varepsilon_0 (d\phi_{sc}/dx)_{x=0}$, and the capacitance of the space charge layer, $C_{sc}$, can now be determined as follows:

$$C_{sc} = \left|\frac{dQ_{sc}}{d\Delta\phi_{sc}}\right| = \left(\frac{\epsilon_r \epsilon_0 e^2 N_D}{2k_B T}\right)^{1/2} \left|\left(\exp\left(\frac{e\Delta\phi_{sc}}{k_B T}\right) - 1\right)\right| \left[\exp\left(\frac{e\Delta\phi_{sc}}{k_B T}\right) - \frac{e\Delta\phi_{sc}}{k_B T} - 1\right]^{-1/2} \quad (8)$$

where $C_{sc}$ is always positive. Equation (8) shows that the capacitance of the space charge layer depends on the total band bending, $\Delta\phi_{sc}$. It is now convenient to simplify equation (8) for two specific cases: (i) accumulation of electrons at the surface with a band bending larger than $3k_BT$ (see Figure 5a), and (ii) depletion of surface electrons with a band bending larger than $3k_BT$ (at room temperature $k_BT$ = 25 meV):

$$e\Delta\phi_{sc} > 3k_BT : C_{sc} = \left(\frac{\epsilon_r \epsilon_0 e^2 N_D}{2k_B T}\right)^{1/2} \exp\left(\frac{e\Delta\phi_{sc}}{2k_B T}\right) \quad (9a)$$

$$e\Delta\phi_{sc} < -3k_BT : C_{sc} = \left(\frac{\epsilon_r \epsilon_0 e^2 N_D}{2k_B T}\right)^{1/2} \left(-\frac{e\Delta\phi_{sc}}{2k_B T} - 1\right)^{-1/2} \quad (9b)$$

Note that $\Delta\phi_{sc}$ is positive in the case of accumulation and negative in the case of depletion. Under accumulation conditions, the capacitance of the space charge layer increases exponentially with the band bending. We will return to the accumulation case in later sections.

Under depletion conditions, $C_{sc}$ has a square root dependence on the band bending and if $C_{sc}^{-2}$ is plotted versus $\Delta\phi_{sc}$ a straight line is obtained and the donor density can be obtained from the slope. This relation is called the Mott-Schottky equation and it is used extensively to determine both the potential at which the bands are flat and the dopant density of the semiconductor. For typical values of dopant density and band bending, the capacitance of the space charge layer is in the range from 10 nF cm$^{-2}$ to 100 nF cm$^{-2}$. Since the capacitance is not strongly dependent on the band bending (see equation (9b)), this value gives a good indication of the low capacitance of the semiconductor space charge layer.

### Helmholtz Layer Capacitance

The Helmholtz layer is analogous to a parallel-plate capacitor where the charge on each plate is separated by a thin dielectric layer. In this case, the capacitance is equal to $(\varepsilon_r \varepsilon_0 / d)$, where $d$ is the thickness of the layer and $\varepsilon_r$ is the dielectric constant of the solvent. The thickness of the solvent layer is approximately equal to the diameter of a water molecule, which is about 6 Å. The dielectric constant of water is about 80, however, this value is much lower for the water layer close to the surface. In this case, the water molecules are strongly polarized in a large electric field (if $\Delta\phi_H$ = 0.3 V and $d$ = 6 Å; the field is $5 \times 10^6$ V cm$^{-1}$) and a value of about 7 for $\varepsilon_r$ is more appropriate. This leads to a value of about 10 $\mu$F cm$^{-2}$ for the Helmholtz layer capacitance, $C_H$. It is evident that the capacitance of the Helmholtz layer is generally much larger than that of the semiconductor space charge layer. In practice, the capacitance of the electric double layer in the solution is more complicated than described above (see Ref. (8)). The most important deviation is caused by (specific) adsorption of charged species to the surface: adsorbed molecules are closer to the surface and they affect the bonding structure and, hence, the energetics of the surface.

### Influence of Adsorption

Up to this point, we have not discussed the absolute energetic position of the band edges at the surface which is an important factor in determining the charge transfer properties of semiconductor electrodes. The Nernst potential of a redox couple is usually given versus the standard reversible hydrogen electrode (*SHE*), which corresponds to the potential of the $H^+/H_2$ redox couple in a 1 M $H^+$ solution at ambient temperature and pressure. SHE is defined as 0 V and has an energy with respect to the vacuum level of about −4.5 eV. In principle, one should be able to use the electron affinity of the semiconductor, however, the semiconductor energetics are strongly influenced by the properties of the electrified interface and the composition of the electrolyte solution. Therefore, the energetic positions of the band edges of semiconductor electrodes in solution are usually also expressed versus the SHE reference level.

In aqueous solutions it is found that the position of the band edges of many semiconductors is dependent on the pH of the solution: at high pH the band edges are shifted to higher energies (i.e. more negative potential versus the reference potential) than at low pH. This suggests that the surface charge is affected by specific adsorption of either $OH^-$ or $H^+$, which is translated into a dependence of the potential drop over the Helmholtz layer on pH. In many cases, the potential drop over the Helmholtz layer and, hence, the energy of the band edges at the surface are found to shift by 60 mV per pH unit. This dependence is observed both on metal oxide semiconductors ($TiO_2$, ZnO) and on silicon and III-V compound semiconductors. The latter is usually explained by assuming the presence of a very thin oxide layer on the semiconductor surface when immersed in solution (see Ref. (9), Chapter 2).

**Electrochemical Cell Impedance.** An electrochemical cell usually consists of a working (*WE*), a reference (*RE*), and a counter electrode (*CE*). The reference electrode is designed to have a large impedance so that there is no current flow and the potential remains constant. In order to allow for current flow, a counter electrode is utilized which usually consists of a platinum mesh with a large surface area. The potential of the working electrode is controlled with respect to the constant potential of the reference by adjusting the potential difference between WE and the CE using a potentiostat.

Figure 4 shows a simple electrical equivalent circuit which will be used as a starting point to describe the electrical properties of semiconductor/electrolyte solution interfaces. The circuit consists of a capacitance due to the semiconductor space charge layer, $C_{sc}$, in series with a Helmholtz layer capacitance, $C_H$, and parallel to the impedance associated with charge transfer (i.e. direct current flow) across the interface, $Z_{CT}$. The resistor, $R_b$,

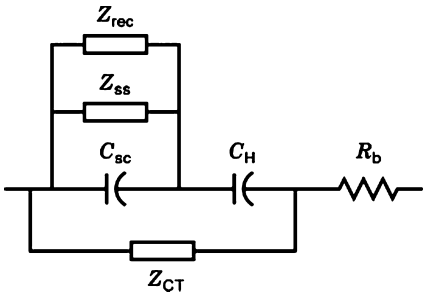


**Figure 4.** Equivalent electrical circuit for a semiconductor/electrolyte solution interface. $C_{sc}$ and $C_H$ are the capacitances of the semiconductor and the Helmholtz layer, respectively. $Z_{CT}$ represents the impedance for charge transfer, and $Z_{ss}$ and $Z_{rec}$ correspond to the impedance associated with surface states and recombination centers. $R_b$ is the uncompensated resistance due to the solution, leads, and contacts.

represents the resistance arising from leads, contacts, solution, and the semiconductor bulk. The impedance of the counter electrode can be excluded since a reference electrode is utilized as a potential probe. The impedances $Z_{ss}$ and $Z_{rec}$ correspond to surface processes which will be discussed later.

It is instructive to consider the situation where there is no charge transfer across the interface and no surface state or recombination processes: in this case, the total cell impedance, $Z_t$, can be evaluated using only the capacitances and the resistances involved:

$$Z_t = R_b + (i\omega C_t)^{-1} \tag{10a}$$

$$C_t = ({C_{sc}}^{-1} + {C_H}^{-1})^{-1} \tag{10b}$$

where $C_t$ is the total capacitance, $i = \sqrt{-1}$, and $\omega$ is the angular frequency of the potential modulation, at which the impedance is measured. In the previous section it was shown that the capacitance of the space charge layer under depletion conditions is much smaller than that of the Helmholtz layer and, hence, the total capacitance is almost equal to that of the space charge layer. In this case, the impedance of the electrochemical cell is dominated by the semiconductor side of the interface. Under accumulation conditions, the value of space charge layer capacitance may become close to that of the Helmholtz layer, and $C_t$ may not be equal to $C_{sc}$; this situation will be discussed in detail in the last section.

When a potential difference is applied between the semiconductor electrode and the solution, the potential drop over both capacitors at the semiconductor/electrolyte solution interface will be affected due to a redistribution of charge. However, from equation (9b) it is clear that under depletion conditions the main part of the applied potential will be dropped over the space charge layer. This can be illustrated using the following set of relations:

$$\Delta U = \Delta(\Delta\phi_{sc}) + \Delta(\Delta\phi_H) = \frac{\Delta Q_{sc}}{C_{sc}} + \frac{\Delta Q_H}{C_H}$$

$$= \Delta Q\left(\frac{1}{C_{sc}} + \frac{1}{C_H}\right) \tag{11}$$

where $\Delta U$ corresponds to an applied potential step and $\Delta\phi_H$ is the change of the potential drop over the Helmholtz layer. Since $C_{sc}$ is much smaller than $C_H$, equation (11) reduces to $\Delta U \approx \Delta(\Delta\phi_{sc})$. One of the most important consequences of this situation is that upon changing the potential drop between the semiconductor electrode and the solution, the potential drop over the Helmholtz layer remains unchanged and, hence, the conduction and valence band edges at the surface remain fixed at the same energy.

Figure 5 shows the effect of the applied potential on the energy band diagrams of a semiconductor. Under equilibrium or open circuit conditions (Figure 5c), a band bending is present and the measured current is zero. If a negative potential equal to the band bending in equilibrium is applied (Figure 5b), the bands are flat and this potential is called the flat band potential, $U_{fb}$. The flat band potential is an important parameter to measure since the knowledge of $U_{fb}$ allows us to determine the band bending at every applied potential (see equation (11)). If the potential is shifted negative of the flat band potential (Figure 5a), the semiconductor may be in accumulation where the density of electrons (CB) at the surface is larger than in the bulk. This situation is interesting for many systems and we will give an example of the formation of an accumulation layer in the last section. If a positive potential with respect to that at equilibrium is applied (Figure 5d), the band bending increases further and the surface may be either in inversion, where the density of holes (VB) is larger than the density of electrons (CB), or in deep depletion. The impedance corresponding to inversion can be found in Reference (9), Chapter 2.

### Charge Transfer Reactions

A unique feature of semiconductors is that the transfer of charge from or to the semiconductor has to flow through either the valence or the conduction band. The energy of the electron accepting or donating levels of the redox couple in solution, Red/Ox, are also at well defined energies. The equilibrium energy, $E_{redox}$, for a redox couple (the solution "Fermi energy") is given by the Nernst equation:

$$E_{redox} = -e\left[U^0_{redox} + \frac{k_B T}{ne}\ln\left(\frac{c_{ox}}{c_{red}}\right)\right] \tag{12}$$

where $U^0{}_{redox}$ is the standard Nernst potential of the couple, $n$ is the number of electronic charges involved in the reaction, and $c_{ox}$ and $c_{red}$ are the concentrations of Ox and Red, respectively. Nernst potentials of redox couples can be obtained from literature (13). An example of electron transfer to a redox couple in the solution is the reduction of molecule Ox to molecule Red (note that Ox and Red have a different net charge, which is left out in this notation):

$$Ox + ne^- \prod Red \tag{13}$$

In practice, however, this is a more complex reaction than suggested by equation (13); molecule Ox is surrounded by solvent and electrolyte molecules which are oriented in such a way as to accommodate for the charge of the molecule. For Ox to accept an electron, this so-called solvation shell needs to be adapted to the electronic configuration of Red. This process requires an energy, called the reorientation energy, $\lambda$. The same reasoning holds for the reverse process where Red is oxidized to Ox. As a conse-

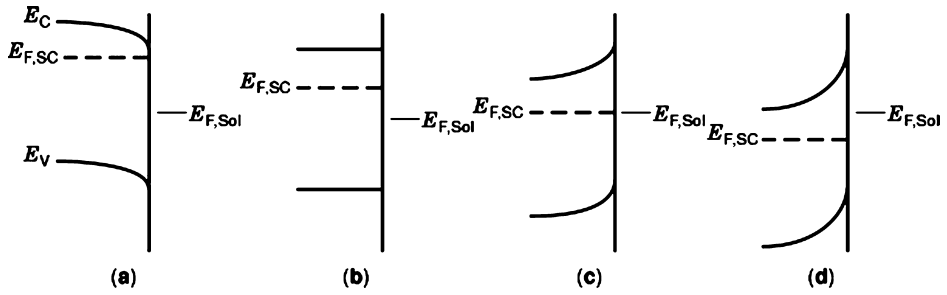


**Figure 5.** In equilibrium, the Fermi energies of an *n*-type semiconductor and the solution are the same. As illustrated in (c), a band bending is usually present in the semiconductor. Upon applying a positive potential (d), the band bending increases, and the semiconductor is in deep depletion or inversion. Inversion corresponds to the situation where at the surface, the density of holes in the valence band is larger than the density of electrons in the conduction band. Upon applying a negative potential equal to the band bending with respect to the situation in (c), the valence and conduction bands are flat and, in this case (b), the applied potential corresponds to the flat band potential, $U_{fb}$. Upon applying an even more negative potential (a), the semiconductor may be in accumulation, corresponding to the situation where the density of electrons at the surface is larger than in the bulk.

quence, the most favorable energies of Ox and Red in order to be involved in a charge transfer process, $E_O$ and $E_R$, are separated by about $2\lambda$ (assuming the process is symmetric; i.e., $E_O$ is $\lambda$ above the Nernst potential and $E_R$ is $\lambda$ below). $E_O$ and $E_R$ are not discrete energy levels, however, due to thermal vibrations in the solvation shell leading to a probability distribution of the energy of Ox and Red; the corresponding distribution function has a Gaussian shape as shown in Figure 6a. For a mathematical treatment of the energy diagram of the solution we refer to Reference (13). The width of the distribution function depends on the magnitude of $\lambda$ which can vary significantly for different redox couples. For example, the reorientation energy of the $Fe^{2+}/Fe^{3+}$ couple is about 1 eV while for the strongly complexed couple $Fe(CN)_6^{4-}/Fe(CN)_6^{3-}$, $\lambda$ is only about 0.5 eV.

The electron transfer process corresponds to the isoenergetic tunneling of an electron from the semiconductor to the solution or vice-versa. As a consequence, electron transfer can only take place if, at an energy $E$, empty levels are present at one side of the interface and filled levels at the other side. For instance, in order to transfer an electron from the conduction band of the semiconductor to an Ox molecule in solution, there must be empty Ox levels at the energy of the conduction band edge at the surface. Figure 6b shows the redox potential of various couples with respect to the band diagram for silicon (at pH 7). For *n*-type silicon in the dark, electrons from the conduction band can be transferred to the solution to reduce water molecules and the oxidized forms of the redox couples shown in Figure 6b. Electrons from the valence band can be transferred to the solution and reduce species such as $Fe^{3+}$. This process is usually called hole injection into the valence band. Under illumination, holes in the valence band are generated and hole transfer to species such as $Fe(CN)_6^{4-}$ can occur. Photogenerated holes can also oxidize the semiconductor itself, which is an important side-reaction that can strongly affect both the electrical and optical properties of the semiconductor/electrolyte boundary. Similar reasoning can be applied for *p*-type silicon, where the majority carriers are holes in the valence band.

The current corresponding to these processes is determined by the density of electrons and holes at the surface,

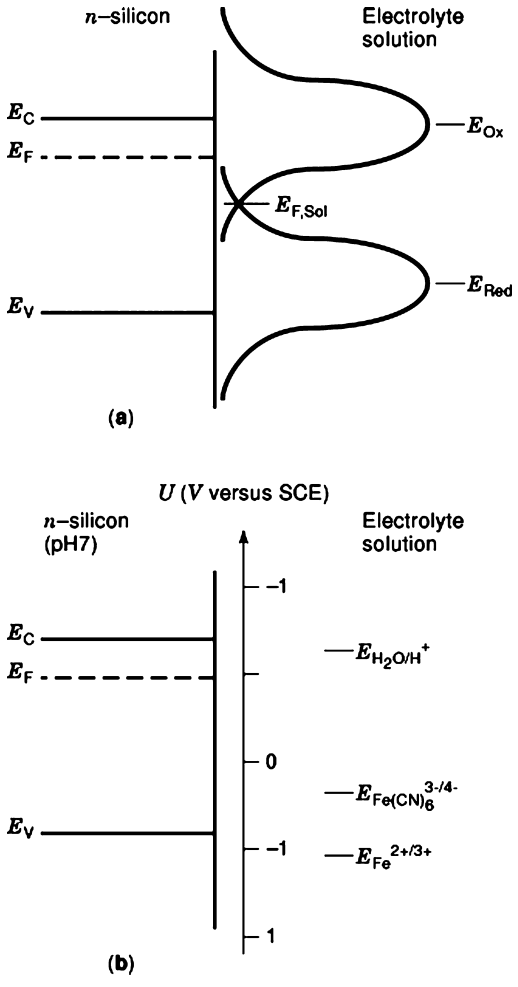


**Figure 6.** The Gaussian shape of the probability function of the energy of redox species in the solution is illustrated in (a). The reorientation energy, $\lambda$, is 0.45 eV in this figure, which is a relatively small value. Figure (b) shows the redox energies of various redox couples and an energy diagram for *n*-type silicon in aqueous solution of pH 7. Note that band diagrams for semiconductors always represent energies; the potential axis versus the saturated calomel reference is included as it is more convenient for the interpretation of experimental results.

the concentration of Red and Ox, and a rate constant that incorporates tunneling constants and the overlap integral of the density of empty and filled levels. In order to understand the current–potential curves of semiconductors in solution it is important to realize that the applied potential mainly affects the band bending in the semiconductor, as described above. In this simple model, the energy of the band edges at the surface and the overlap integral are independent of the applied potential. As a consequence, the current–potential curve mainly reflects the potential dependence of the density of electrons or holes at the surface.

### Examples

Figure 7 shows an example of the current–potential characteristics *n*-type silicon in a 1 M HF solution in the dark. The redox couple of importance in this case is the $H^+/H_2$ couple. The energetics of this case can be inferred from Figure 6b; note that the pH of the solution is 2, hence, both the redox potential and the band edges are shifted to more positive potentials than the values shown in Figure 6b. The formation of an oxide layer is avoided by the presence of HF in the solution. The current–potential curve shows that at positive potentials the current is small; this is due to the absence of holes in the valence band. At potentials more negative than −0.7 V(SCE), a cathodic current is observed which is due to the reduction of $H^+$ to hydrogen. It can be concluded that at −0.7 V, the density of electrons at the surface has become sufficiently high to generate a measurable current. The density of electrons (CB) at the surface, $n_s$, can be described by the Boltzmann equation (Equation (5)): $n_s$ is equal to the donor density at the flat band potential and decreases upon shifting the potential to more positive values. However, from the current–potential curve the flat band potential cannot be obtained since the value for the rate constant for the process is not known. Therefore, impedance measurements as a function of the applied potential must be performed to determine the flat band potential. As described above, the capacitance of the silicon electrode is given by the Mott-Schottky equation (equation (9b)). Using the results from the previous paragraphs, equation (9b) can be converted to a more convenient form:

$$\frac{1}{C^2} = \frac{2}{\epsilon_r \epsilon_0 e N_D}\left(U - U_{fb} - \frac{k_B T}{e}\right) \qquad (14)$$

where $C$ is the measured capacitance, and $U$ and $U_{fb}$ are the applied potential and the flat band potential versus the reference electrode, respectively. We will use the saturated calomel electrode (*SCE*) as reference which is 0.24 V positive with respect to the standard hydrogen electrode. Figure 7 shows that the plot of $C_p^{-2}$ versus potential is linear at positive potentials, and the flat band potential is determined to be −0.45 V(SCE). The measured impedance is analyzed on the basis of a parallel (RC) circuit in series with $R_b$, and the measured capacitance is denoted $C_p$. Under the conditions that $C_H >> C_{sc}$, that $Z_{CT}$ is purely resistive, and in the absence of surface states or recombination processes, $C_p = C_{sc}$ (see Fig. 4 and Eq. 11). The donor density is determined from the slope to be $5 \times 10^{13}$ cm$^{-3}$ which corresponds to a resistivity of 90 Ω cm, in excellent agreement with four point probe measurements. Using equation

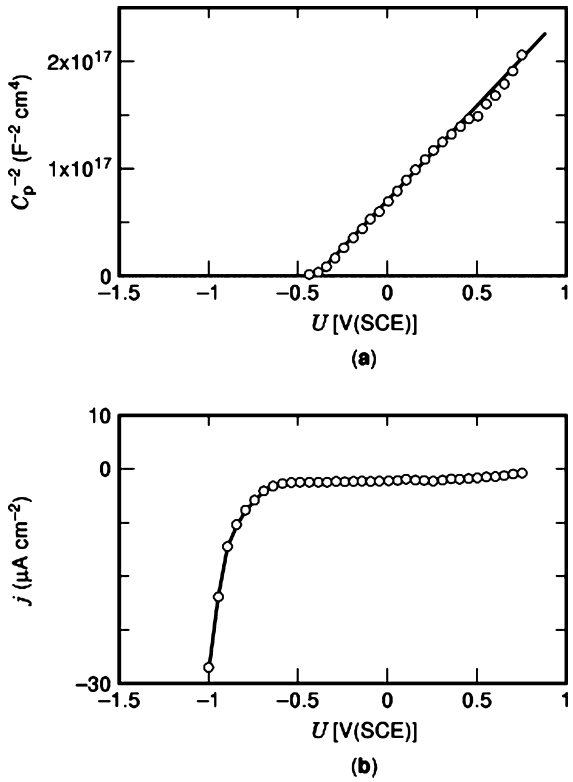


**Figure 7.** The Mott-Schottky plot (a) and the current–potential curve (b) for *n*-type silicon ($N_D = 5 \times 10^{13}$ cm$^{-3}$) in 1 M $NH_4F$ at pH 9 in the dark. The donor density was determined from the slope, and the flat band potential is −0.45 V(SCE). The modulation frequency and amplitude were 10 kHz and 10 mV, respectively. The rectifying characteristics of the semiconductor is observed in (b) as the current at positive potentials is small due to the absence of holes in the valence band. The forward current at potentials more negative than −0.6 V(SCE) is due to the reduction of water to hydrogen, involving the transfer of electrons from the conduction band.

(2a), the position of the conduction and valence band edges at the surface are found to be −0.74 eV and 0.38 eV (versus SCE), respectively. From these results the energetic scheme shown in Figure 6b can be constructed, and kinetic parameters such as the rate constants for the involved processed can be obtained.

In Figure 8, the current–potential curves for *n*-type silicon in 0.1 M $K_4Fe(CN)_6$ + 0.5 M KCl + 1 M $NH_4F$, both in the dark and under illumination are shown. The $K_4Fe(CN)_6$ is added to stabilize the electrode. As was shown in Figure 6b, holes in the valence band can be transferred to $Fe(CN)_6^{4-}$ in solution preventing extensive oxidation of the silicon surface under illumination. At positive potentials, a current plateau is observed where the current is limited by the light intensity, that is by the generation rate of holes in the valence band. From comparison with the current in the dark it is clear that the photocurrent is much larger than the dark current. The theoretical shape of the photocurrent potential curve can be obtained from the Gärtner equation

(see Ref. (9), Chapter 4):

$$j_p = eI_0\left[1 - \frac{1}{1+\alpha L}\exp(-\alpha W)\right] \qquad (15)$$

where $j_p$ is the photocurrent, $I_0$ is the light intensity at the interface, $\alpha$ is the absorption coefficient of the semiconductor, $L$ is the diffusion length of the minority carriers, and $W$ is the width of the space charge layer which depends on the applied potential. This expression assumes negligible recombination of holes and electrons in the space charge layer and at the surface and that hole transfer to the solution is very fast. For silicon, the minority carrier diffusion length is very large so that $\alpha L >> 1$. As a consequence, even at the flat band potential where $W = 0$, the photocurrent is almost equal to the saturation value. Figure 8 shows the theoretical photocurrent–potential curve for silicon (dotted line) under the assumptions of equation (15). The large discrepancy between experiment and theory is explained by two processes: first, the surface has been oxidized and the trapped positive charges in the thin interfacial oxide layer have shifted the band edges and, secondly, the recombination rate at the surface is large. Recombination of photogenerated holes with electrons in the conduction band results in a decrease of the observed photocurrent. If all holes recombine, the photocurrent is zero. Surface recombination preferably occurs at centers in the band gap, where holes (VB) and electrons (CB) are subsequently trapped. The recombination rate increases with decreasing band bending as the density of electrons at the surface increases (see equation (5)). Note that recombination can also take place in the dark on an $n$-type semiconductor when a hole injecting species such as $Fe^{3+}$ is present. Figure 8 also shows the Mott-Schottky plots in the dark (a) and under illumination (b). The band edges have shifted to lower energy (i.e. more positive potentials) under illumination confirming the presence of an interfacial layer or positively charged oxidation intermediates. If the shift of the band edges is taken into account, there is still a discrepancy between the theoretical and experimental results, indicating that recombination also plays a role.

In summary, although current–potential and Mott-Schottky plots are the basis for all research in semiconductor/electrolyte boundary systems, they are not sufficient to completely understand the electrical properties of semiconductor/electrolyte interfaces. In the following section we will discuss techniques to determine the influence of surface states, recombination, and the presence of an interfacial layer.

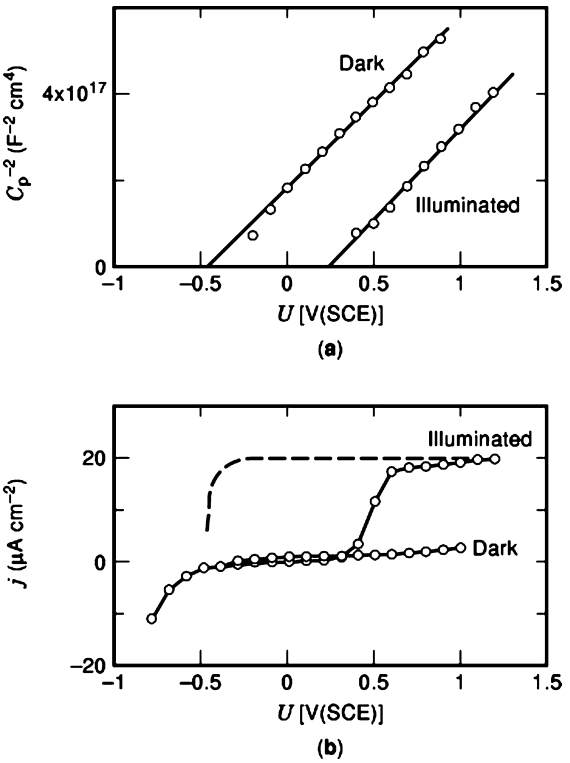


**Figure 8.** Mott-Schottky plots (a) and current–potential curves (b) for $n$-type silicon in 0.1 M $K_4Fe(CN)_6$ + 1 M $NH_4F$ at pH 9, both in the dark and under illumination. The modulation frequency and amplitude were 10 kHz and 10 mV (rms), respectively. Under illumination, a current plateau is observed at positive potentials where the photocurrent is determined by the light intensity. The dotted curve shows the theoretical current–potential curve as calculated from equation (14), assuming the ideal situation where the band edges do not shift under illumination, and that recombination at the surface does not occur. Figure (a) shows that the band edges have shifted under illumination, indicating the presence of an interfacial layer and/or trapped positive charge in oxidation intermediates. The flat band potential under illumination is 0.25 V(SCE), and (b) shows that the photocurrent onset is at 0.4 V(SCE), suggesting that recombination also occurs.

## MODULATION TECHNIQUES

Modulation techniques provide a powerful tool to study the kinetics of processes occurring at the semiconductor/electrolyte boundary. In general, a small modulation is superimposed on a *dc* signal and the modulated response is measured. The impedance, $Z$, is then defined as the modulated signal divided by the modulated response. Both the amplitude of the response and a possible phase shift contain kinetic information and, therefore, the results are usually expressed in a complex number notation using the real and imaginary parts of the impedance. The corresponding admittance is defined as $Z^{-1}$. The results of impedance techniques are interpreted on the basis of linear models, i.e., that the response is linearly related to the perturbation. Requirements of the linear systems theory are that the system is stable, the response is caused by the perturbation, and that the amplitude is sufficiently small. For a detailed treatment of impedance techniques in electrochemistry, the reader is referred to Reference (14). In this section, we will address three important modulation methods: electrochemical impedance spectroscopy (*EIS*), intensity modulated photocurrent spectroscopy (*IMPS*), and potential modulated microwave reflectivity spectroscopy (*PMMRS*).

In EIS, a sinusoidal potential signal of small amplitude $\tilde{U}$, is superimposed on the applied potential. The modulated current at the same frequency, $\tilde{j}$, is then measured and the electrochemical impedance is defined by $\tilde{U}/\tilde{j}$.

Electrochemical impedance spectroscopy, therefore, gives information on processes resulting in a (modulated) current in the external circuit. The impedance is measured as a function of the modulation frequency and time constants for various processes can thus be determined. For many experiments in semiconductor electrochemistry, impedance spectroscopy is performed as a function of the applied potential, for instance, to generate a Mott-Schottky plot. In IMPS, photoelectrochemical processes are investigated by superimposing a small modulated light intensity on a base light intensity and measuring the modulated photocurrent. This technique is very useful to determine rate constants for charge transfer reactions, but also provides quantitative information on the recombination of photogenerated charge carriers and the majority carriers at the semiconductor/electrolyte boundary. IMPS gives, in principle, the same information as time-domain experiments used extensively in semiconductor physics and photoelectrochemistry. However, IMPS has the advantage that results can be interpreted in terms of the linear systems theory and that the base light intensity dependence can be easily studied. In PMMRS, a small sinusoidal potential modulation is superimposed on the applied potential as in EIS, but now the modulated microwave reflectivity is measured. This is achieved by exposing the semiconductor to a constant microwave intensity; the reflected microwave intensity at the frequency of the potential modulation is then determined.

Up to this point, the influence of specific surface-related processes has not yet been considered. In the following paragraphs, we provide a quantitative treatment of the electrochemical impedance due to various kinds of electrically active surface states and comparison to experimental data. IMPS and PMMRS are discussed in detail and examples of the characterization of surface-related processes using these techniques are given.

### Electrochemical Impedance Due to Surface States

The surface of a semiconductor is usually associated with the presence of surface states which are usually located energetically in the bandgap. These states can act as electronic donors or acceptors, or as recombination centers. The influence of the presence of electrically active states in the bandgap of semiconductors is treated in detail in Reference (15).

We will use a kinetic approach to calculate the effective impedances due to the presence and interactions of various types of surface states which are illustrated schematically in Figure 9. First, surface states that trap and de-trap electrons from the conduction band of an $n$-type semiconductor will be considered. Since these states only interact with the majority carriers in the conduction band they are active in the dark. Figure 9a schematically shows the kinetic interactions between the surface states and the conduction band, indicated by arrows which are labeled with their respective rate constants $k_1$ and $k_2$. The interactions considered here can be written in the following 'reaction' schemes:

$$SS^0 + e^-(CB) \xrightarrow{k_1} SS^- \tag{16a}$$

$$SS^- \xrightarrow{k_2} SS^0 + e^-(CB) \tag{16b}$$

In impedance measurements, a small harmonic perturbation $\tilde{U} = U_a \exp(i\omega t)$ is superimposed upon the steady-state applied potential, $U$, where $U_a$ is the modulation amplitude and $\omega$ is the angular frequency of the modulation. In the following, we will denote all modulated quantities by '$\sim$.' By using a small perturbation, the modulated parameters can be approximated by the first terms of their respective Taylor expansions. The potential modulation results in a modulated density of electrons at the surface, $n_s + \tilde{n}_s$. Equation (5) can be adapted to the following, more convenient expression for $n_s$:

$$n_s = N_D \exp\left[-\frac{e}{k_B T}(U - U_{fb})\right] \tag{17}$$

where $U$ is the applied potential and $U_{fb}$ is the flat band potential, both expressed versus SCE. In this equation it is assumed that the potential drop over the Helmholtz layer is independent of the applied potential. The modulated density of electrons at the surface at the applied potential can be obtained by taking the first derivative of $n_s$:

$$\tilde{n}_s = \frac{dn_s}{dU}\tilde{U} = -\frac{e}{k_B T} n_s \tilde{U} \tag{18}$$

The modulation of $n_s$ leads to a modulated occupancy of the surface states, hence, a time-dependent rate equation can be written as follows:

$$\begin{aligned}\frac{ds^-}{dt} = \frac{d\tilde{s}^-}{dt} &= k_1(n_s + \tilde{n}_s)(s^0 + \tilde{s}^0) - k_2(s^- + \tilde{s}^-) \\ &= k_1 n_s \tilde{s}^0 + k_1 s^0 \tilde{n}_s - k_2 \tilde{s}^-\end{aligned} \tag{19}$$

where $s^-$ and $s^0$ are the density of 'filled' and 'empty' surface states, respectively. Since the system is always close to the steady-state situation, terms that contain products of two modulated quantities or do not contain a modulated parameter are omitted. As $s^-$ is modulated with the same period as $U$, $\tilde{s}^- = s^-_a \exp[i(\omega t + \theta)]$ (where $\theta$ corresponds to a phase shift) and, consequently, $d\tilde{s}^-/dt = i\omega\tilde{s}^-$. Substitution into equation (19) leads to:

$$\tilde{s}^- = -\frac{e}{k_B T} n_s \frac{k_1 s^0}{i\omega + k_2 + k_1 n_s}\tilde{U} \tag{20}$$

Using equations (17–20) the modulated current associated with trapping and de-trapping of conduction band electrons in surface states can be written as:

$$\tilde{j} = -e\frac{d\tilde{s}^-}{dt} = \frac{e^2}{k_B T} k_1 n_s s^0 \frac{i\omega}{i\omega + k_2 n_s}\tilde{U} \tag{21}$$

The impedance corresponding to trapping and de-trapping of electrons on the surface states is now obtained by dividing the modulated potential by the modulated current:

$$Z = \frac{\tilde{U}}{\tilde{j}} = \frac{k_B T}{e^2}(k_1 n_s s^0)^{-1}\left(1 + \frac{k_1 n_s + k_2}{i\omega}\right) \tag{22}$$

The impedance corresponds to a series equivalent circuit consisting of a resistance $R_s$ and a capacitance $C_s$:

$$R_s = \frac{k_B T}{e^2}(k_1 n_s s^0)^{-1} \tag{23a}$$

$$C_s = \frac{e^2}{k_B T}\left(\frac{k_1 n_s s^0}{k_1 n_s + k_2}\right) \tag{23b}$$

Figure 10a shows the equivalent circuit for the surface states which is in parallel to the space charge layer capacitance (see Figure 4). The total measured capacitance of the system includes the space charge layer capacitance and the surface state capacitance. It is therefore convenient to convert the series equivalent circuit for the surface states into a parallel one with frequency-dependent components. The space charge layer and surface state capacitances are then in parallel, and the sum of the two directly corresponds to the measured capacitance. The frequency-dependent parallel capacitance due to the surface states can be obtained from equation (23) and is given by:

$$C_p^{SS}(\omega) = \frac{e^2}{k_B T}\left(\frac{k_2 k_1 n_s}{\omega^2 + (k_1 n_s + k_2)^2}\right) s_t \tag{24}$$

where $s_t$ is the total density of surface states. Equation (24) shows that the surface state pseudo-capacitance depends on both the applied potential (through $n_s$) and the frequency of modulation. At high frequencies the surface state pseudo-capacitance is proportional to $\omega^{-2}$, while at low frequencies the capacitance approaches a frequency independent value which has a maximum at the potential where $k_1 n_s = k_2$, and $s^0 = s^- = s_t/2$ (Figure 11):

$$C_p^{SS}(\max) = \frac{1}{4}\frac{e^2}{k_B T} s_t \tag{25}$$

From this the total density of dark surface states can be determined. This calculation assumes that the density of surface states is smaller than about $10^{12}$ cm$^{-2}$; a more rigorous analysis is needed when $s_t$ is larger, which can be found in Reference (16).

An example of the presence of electrically active surface states is found for $n$-type silicon (111) in fluoride solutions. Figure 11 shows the measured parallel capacitance, $C_p$, versus the applied potential for $n$-type silicon in I M $NH_4F$ at pH 9 (refer to Figure 7 for the current–potential and Mott-Schottky curves). A capacitance peak is observed which can be ascribed to electrically active surface states at an energy of about 0.4 eV below the conduction band edge. The density of surface states was determined as a function of the pH in 1 M $NH_4F$ solution, and the results are shown in the inset. The density of surface states ranges from a $2 \times 10^{10}$ cm$^{-2}$ at low pH to $1 \times 10^{12}$ cm$^{-2}$ at high pH. The de-trapping rate constant $k_2$ for these states was determined to be about $10^4$ s$^{-1}$ (17).

The merit of this approach is that the kinetic scheme can be easily extended to include more processes such as interaction of surface states with a redox-couple in solution or with holes in the valence band (16). These calculations are beyond the scope of this chapter, but we will briefly discuss the latter possibility in the subsequent section.

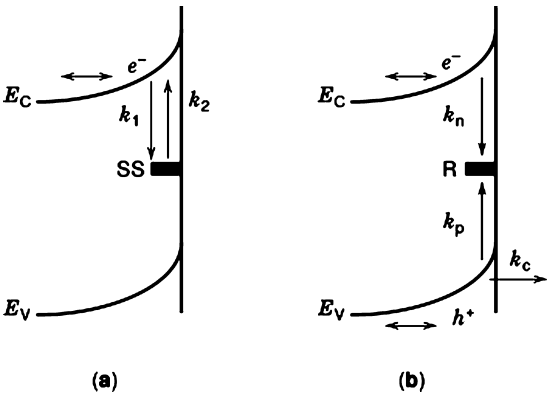


**Figure 9.** The surface states shown in (a) only interact with the conduction band. The trapping and detrapping of electrons on the surface states gives rise to a characteristic electrical impedance, $Z_{ss}$, as shown in Figure 10(a). Recombination centers interact with both the valence band and the conduction band. Recombination occurs by the subsequent trapping of photogenerated holes (or holes injected into an $n$-type semiconductor from an electron accepting solution species such as $Fe^{3+}$ (see Figure 6)) and electrons from the conduction band. The corresponding electrical impedance, $Z_{rec}$, is shown in Figure 10(b).

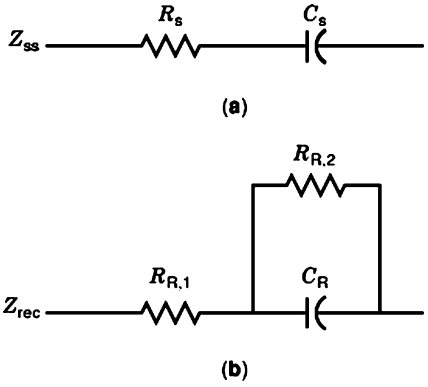


**Figure 10.** The electrical impedance corresponding to surface states interacting with the conduction band only (a), and the electrical impedance due to recombination centers (b). The complete equivalent circuit can be found by placing the impedances $Z_{ss}$ and $Z_{rec}$ in the circuit shown in Fig. 4.

### Electrochemical Impedance Due to Recombination

Another important type of surface states are recombination centers. The impedance due to surface recombination can be obtained in a similar fashion as discussed above for the case of surface states which only interact with majority carriers (see Ref. (18)). The recombination reactions at a recombination center R can be written as (see Figure 9b):

$$R^+ + e^-(CB) \xrightarrow{k_n} R^0 \tag{26a}$$

$$R^0 + h^+(VB) \xrightarrow{k_p} R^+ \tag{26b}$$

where $R^+$ and $R^0$ are the positively charged and neutral recombination centers, respectively, and $k_n$ and $k_p$ are the relevant rate constants. The corresponding impedance can be represented by the equivalent circuit shown in Figure 10b. The components of the equivalent circuit are given by:

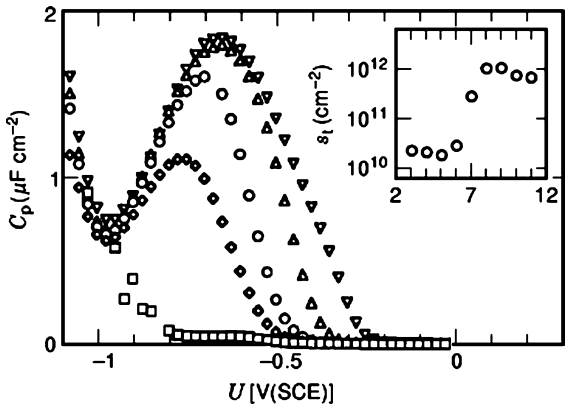


**Figure 11.** The measured parallel capacitance versus applied potential for *n*-type silicon in 1 M $NH_4F$ at pH 9 in the dark at (▽) 10 Hz, (△) 100 Hz, (○) 1 kHz, (◇) 10 kHz, (□) 100 kHz. The modulation amplitude was 3 mV (rms). The density of surface states is determined using equation (24) from the maximum in $C_p$ at −0.6 V(SCE) by subtracting the space charge layer capacitance. The inset shows that the density of surface states in 1 M $NH_4F$ solutions is about $10^{10}$ cm$^{-2}$ at pH < 7 and about $10^{12}$ cm$^{-2}$ at pH > 7. This is related to the formation of a thin oxide layer which is almost completely prevented at low pH due to the high concentration of HF, while at high pH, the concentration of undissociated HF is too low to prevent oxide formation.

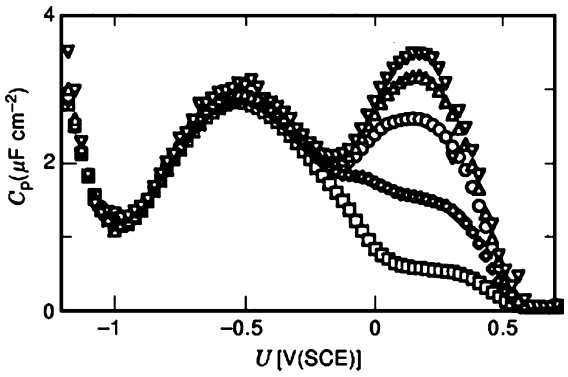


**Figure 12.** The measured parallel capacitance versus applied potential for *n*-type silicon in 0.1 M $K_4Fe(CN)_6$ + 1 M $NH_4F$ at pH 9 under illumination at (▽) 2.15 Hz, (△) 10 Hz, (○) 21.5 Hz, (◇) 46.4 kHz, (□) 100 Hz. The photocurrent in the plateau region was 35 μA cm$^{-2}$ and modulation amplitude was 3 mV (rms). The peak at −0.5 V(SCE) corresponds to surface states interacting with the conduction band only; under illumination, their density has increased by about a factor of two. The peak at 0.2 V(SCE) is due to recombination. The density of recombination centers was determined from the 2.15 Hz curve to be $4 \times 10^{12}$ cm$^{-2}$ using equation (28). The difference in frequency dependence of the responses corresponding to the surface states, and the recombination centers illustrates the difference in kinetics for the two processes involved.

$$R_{R.1} = \left(\frac{e^2}{k_B T} k_n n_s (r_t - r^0)\right)^{-1} \tag{27a}$$

$$R_{R.2} = \left(\frac{e^2}{k_B T} k_p p_s (r_t - r^0)\right)^{-1} \tag{27b}$$

$$C_R = \frac{e^2}{k_B T}(r_t - r^0) \tag{27c}$$

where $r^0$ and $r^+$ are the densities of filled and empty recombination centers, respectively, and $r_t = r^0 + r^+$. Again it is convenient to convert this circuit into a parallel equivalent circuit of frequency dependent elements; the parallel pseudo-capacitance, $C_p{}^R(\omega)$, is given by:

$$C_p^R(\omega) = \frac{e^2}{k_B T}(r_t - r^0)\frac{1}{\left(\frac{r_t}{r^0}\right)^2 + \left(\frac{\omega}{k_n n_s}\right)^2} \tag{28}$$

For low frequencies $C_p{}^R(\omega)$ shows a maximum as a function of the applied potential and the maximum is given by:

$$C_p^R(\max)_{\omega \to 0} = \frac{4}{27}\frac{e^2}{k_B T} r_t \tag{29}$$

It is therefore possible, as for the dark surface states, to determine the density of the recombination centers and the relevant rate constants by impedance analysis.

Figure 12 shows an example for this case. The parallel capacitance is plotted versus the applied potential for *n*-type silicon (111) in 1 M $NH_4F$ + 0.1 M $K_4Fe(CN)_6$ at pH 9 under illumination (refer to Figure 8 for the current–potential and Mott-Schottky curves). In the dark one peak is observed corresponding to surface states (see Figure 11), while under illumination two maxima are found. The peak at 0.2 V can be ascribed to recombination. Analysis of the impedance showed that the two peaks are not associated with recombination at the surface states observed in the dark. The density of the recombination centers was found to increase with increasing light intensity up to a value of about $4 \times 10^{12}$ cm$^{-2}$. A more detailed analysis of these results is provided in Ref. (19).

### Intensity Modulated Photocurrent Spectroscopy (IMPS)

IMPS is a very useful method to determine the kinetic parameters of processes involving minority carriers. In an *n*-type semiconductor the modulation of the incident light intensity will directly affect the surface hole concentration, and the rate constants for hole transfer to the solution and recombination can be determined (19, 20). An interesting point is that (at least as a first order approximation) IMPS will not be influenced by the presence of surface states which only interact with the majority carriers.

We will consider the reaction scheme given in equations (30a,b,c). The recombination process corresponds to reactions (a) and (b); the photocurrent is described by reaction (c):

$$R^0 + h^+(VB) \xrightarrow{k_p} R^+ \tag{30a}$$

$$R^+ + e^-(CB) \xrightarrow{k_n} R^0 \tag{30b}$$

$$Red + h^+(VB) \xrightarrow{k_c} Ox \tag{30c}$$

IMPS measurements are performed at constant applied potential, and the density of electrons at the surface is constant, however, the modulation of the density of holes at

the surface will modulate the occupancy of the recombination centers. The IMPS response is usually represented as an admittance, $\Phi$, which corresponds to the *ac* photon-to-current conversion efficiency. The real and imaginary parts for this scheme can be calculated in a similar way as was shown for the surface states, and are given by:

$$\mathrm{Re}(\Phi) = \mathrm{Re}\left(\frac{\tilde{j}_\mathrm{p}}{\tilde{j}_\mathrm{h}}\right) = 1 - k_\mathrm{n} n_\mathrm{s} \frac{\beta\tau}{\omega^2\tau^2 + 1} \tag{31a}$$

$$\mathrm{Im}(\Phi) = \mathrm{Im}\left(\frac{\tilde{j}_\mathrm{p}}{\tilde{j}_\mathrm{h}}\right) = k_\mathrm{n} n_\mathrm{s} \frac{\beta\tau^2\omega}{\omega^2\tau^2 + 1} \tag{31b}$$

where $j_\mathrm{p}$ is the photocurrent, $j_\mathrm{h}$ is the hole generation current (which is proportional to the light intensity), and symbols denoted by '$\sim$' correspond to the modulated quantities. The parameter $\beta$ describes the ratio between charge transfer and recombination, and $\tau$ is the recombination time constant. $\beta$ and $\tau$ are given by:

$$\beta = \frac{k_\mathrm{p} r^0}{k_\mathrm{p} r^0 + k_\mathrm{c}} \tag{32}$$

$$\tau = [k_\mathrm{n} n_\mathrm{s} + k_\mathrm{p} p_\mathrm{s}(1 - \beta)]^{-1} \tag{33}$$

If all photogenerated holes recombine and the photocurrent observed in the current–potential plot is zero, equations (31a, b) show that a plot of the IMPS response in the complex plane will give a semicircle, with a high frequency limit of 1 and a low frequency limit of 0 on the real axis. This can be explained as follows: at high frequency, the surface hole density is modulated faster than the time constant of the recombination process, and the modulated hole flux through the depletion layer is in phase and equal to the modulated hole generation flux. At lower frequencies, recombination can take place leading to a decreased photocurrent and in the low frequency limit, all generated holes recombine. As a consequence, the observed current in the steady-state current–potential curve is zero. The frequency at the maximum of the semicircle, $\omega_\mathrm{m}$, is equal to $\tau^{-1}$. In most cases, $k_\mathrm{n} n_\mathrm{s} >> k_\mathrm{p} p_\mathrm{s}$, and therefore, $\omega_\mathrm{m}$ is equal to $k_\mathrm{n} n_\mathrm{s}$ and the rate constant for trapping of electrons in recombination centers can be easily determined.

Figure 13 shows an IMPS spectrum for *n*-type silicon in 1 M $NH_4F$ + 0.1 M $K_4Fe(CN)_6$ at pH 9 at a potential of $-0.1$ V where the *dc* photocurrent is zero. As described above, the rate constant for recombination can be determined from the frequency at the apex of the loop. The inset shows the dependence of the recombination rate constant on the applied potential. Upon increasing the electron density (i.e. at more negative potentials) the recombination rate increases exponentially with the applied potential. The plateau in the curve between 0.1 V(SCE) and 0.3 V(SCE) is related to the shift of the band edges taking place in that potential region (19).

The potential dependence of the high frequency value of the admittance $\Phi$ follows the theoretical curve shown in Figure 8, corresponding to equation (15) (after correcting for the shift of the band edges). Thus, at sufficiently high frequency the recombination process cannot follow the modulation of the light intensity and the "ideal" current–potential curve is obtained.

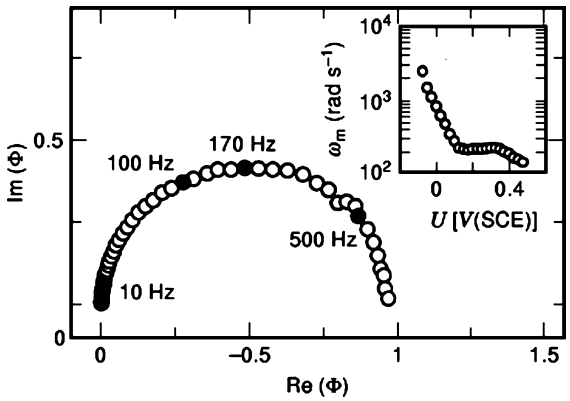


**Figure 13.** IMPS spectrum for *n*-type silicon in 0.1 M $K_4Fe(CN)_6$ + 0.5 M KCl at pH 9 at 0 V(SCE) at a *dc* light intensity corresponding to 15 $\mu$A cm$^{-2}$. The light source was a red LED ($\lambda$ = 650 nm), and its intensity was modulated by modulating the driving current; the modulation amplitude corresponded to 1 $\mu$A cm$^{-2}$ (rms). At high frequencies, the quantum efficiency is equal to 1 while at low frequencies it goes to zero. The *dc* photocurrent was zero at this potential. The recombination time constant, $k_\mathrm{n}$, can be determined using equation (32). The frequency at the apex of the loop is 170 Hz, and the band bending, which determines $n_\mathrm{s}$ [see equation (16) ], is 0.15 eV resulting in a value for $k_\mathrm{n}$ of about $10^{-9}$ cm$^3$ s$^{-1}$. The inset shows the frequency at the apex of the loop as a function of the applied potential. Upon shifting the potential negative, $\omega_\mathrm{m}$ increases exponentially, confirming the increase of the recombination rate with decreasing band bending.

### Potential Modulated Microwave Reflectivity

Potential Modulated Microwave Reflectance Spectroscopy (*PMMRS*) is a relatively new technique for the characterization of semiconductor/electrolyte interfaces (21). In PMMRS, the applied potential is modulated, as in EIS, but now the modulated microwave reflectivity is measured. The experimental set-up required for PMMRS can be found in Reference (21). PMMRS is especially useful in the potential regions where the electrochemical impedance is dominated by surface state processes or charge transfer. The microwave reflectivity only probes the space charge layer of the semiconductor, and hence the band bending, in potential regions where surface states are active or charge transfer takes place.

The microwave reflectivity, $R$, of a semiconductor is proportional to its conductivity, $\sigma$. If the applied potential is modulated, the conductivity is also modulated through the modulated band bending and, hence, the electron density. If a small potential modulation, $\tilde{U}$, is used, the microwave reflectivity, $\tilde{R}$, for an *n*-type semiconductor (neglecting the contribution of minority carriers) is given by:

$$\tilde{R} = S\tilde{\sigma} = S\mu_\mathrm{n} e\tilde{n} \tag{34}$$

where $S$ is the sensitivity factor, $\tilde{n}$ is the modulated electron density in the semiconductor (which corresponds to the modulated density of electrons in the space charge layer) in units of cm$^{-2}$, $\mu_\mathrm{n}$ is the mobility of the electrons, and $e$ is the electronic charge. By solving the Poisson equation the

modulated microwave reflectivity is found to be:

$$\tilde{R} = S\mu_n C_{sc}\Delta\tilde{\phi}_{sc} \tag{35}$$

where $\Delta\tilde{\phi}_{sc}$ is the modulated band bending and $C_{sc}$ is the space charge layer capacitance (see equations (8) and (9)). The admittance, $Y_R$, of the microwave reflectivity is now defined as:

$$Y_R = \frac{\tilde{R}}{\Delta\tilde{\phi}_{sc}} = S\mu_n C_{sc} \tag{36}$$

The electron density increases as the applied potential is made more negative and, as a consequence, $\tilde{R}$ is expected to be 180° out of phase with the potential modulation. Therefore, in complex plane representation, the real component of $Y_R$ has a negative value while the imaginary component of $Y_R$ is negligible. Equations (34–36) reflect that localized electrons trapped in surface states, recombination centers, or in an interfacial layer do not affect the microwave reflectivity since they have a very low mobility. Note that the equilibration process of the majority carriers in the space charge region of crystalline semiconductors is much faster than the typical frequency of the potential modulation used in PMMRS and, therefore, the microwave response does not provide information on electron transport in the bulk of the semiconductor.

Equation (36) shows that, under depletion conditions (where $\tilde{U} = \Delta\tilde{\phi}_{sc}$) a Mott-Schottky plot can be constructed by plotting $|Y_R|^{-2}$ versus the applied potential. At potentials close to or negative of the flat band potential, the semiconductor capacitance is given by equations (8) and (9a). As $C_{sc}$ increases to values close to that of the Helmholtz layer, the applied potential and the applied modulated potential are partitioned over the space charge layer and the Helmholtz layer ($\tilde{U} \neq \Delta\tilde{\phi}_{sc}$ and $\Delta U \neq \Delta\phi_{sc}$). As a consequence, the measured microwave reflectivity admittance is modified. Assuming the simplest case where $Z_{CT}$ corresponds to a large resistor and neglecting $Z_{ss}$ and $Z_{rec}$, it can be shown that the measured microwave reflectivity admittance, $Y_{R,m}$, is given by:

$$Y_{R,m} = \frac{\tilde{R}}{\tilde{U}} = S\mu_n C_{sc}\frac{C_H}{C_{sc}+C_H} \tag{37}$$

Equation (37) shows that in the limiting case where $C_{sc} > C_H$, the measured microwave reflectivity admittance is determined by $C_H$.

Figure 14 shows plots of the measured capacitance and the modulus of $Y_R$ versus the applied potential of $n$-type silicon (111) in a 0.01 M $NH_4F$ solution (pH 6.8). Note that $|Y_R| = -\mathrm{Re}(Y_R)$ since $\mathrm{Im}(Y_R) \to 0$. At potentials between −0.2 and −0.6 V where surface states are electrically active, the measured capacitance corresponds to the filling and emptying of surface states. The $|Y_R|$ versus potential plot, on the other hand, follows the Mott-Schottky equation, showing that the microwave reflectivity method is not affected by the presence of surface states. In a narrow potential region just negative of the flatband potential (−0.3 V), the increase in the $|Y_R|$ signal is exponential with an inverse slope of 160 mV/decade. The expected potential dependence of the capacitance for an accumulation layer is 120 mV/decade (see equation (9a)) indicating that

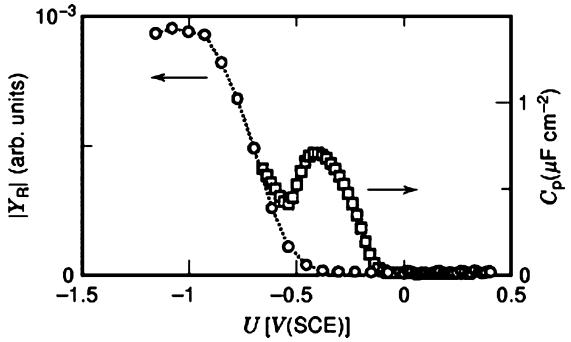


**Figure 14.** The measured parallel capacitance (□) and the modulus of the microwave reflectivity admittance (○) versus the applied potential for $n$-type silicon in 0.01 M $NH_4F$ at pH 6.8. The modulation amplitudes and frequencies were 10 mV (rms) and 20 Hz for the capacitance measurements and 20 mV (rms) and 10 Hz for the microwave reflectivity experiments, respectively. A peak corresponding to surface states is observed in the capacitance plot at −0.4 V(SCE), while the microwave reflectivity admittance follows the Mott-Schottky relation. This confirms that the microwave reflectivity method only probes the semiconductor space charge region and is not affected by electrically active surface states. At potentials just negative of the flat band potential ($U_{fb}$ = −0.5 V(SCE)), the microwave reflectivity signal increases exponentially with the potential which is indicative of accumulation (see Figure 5(a)).

a small fraction of the applied potential is dropped over the Helmholtz layer. This suggests that the semiconductor capacitance has increased to a value close to that of the Helmholtz layer. At potentials negative of −1 V(SCE), the applied potential is mainly dropped over the Helmholtz layer and the microwave reflectivity admittance saturates at a constant value. In this potential region, the band edges are no longer fixed but shift to higher energy upon applying a more negative potential.

## SUMMARY

The semiconductor – electrolyte interface is described both in the dark and under illumination. The energy band structure of the semiconductor, and the energetics of interface formation upon introduction of a semiconductor surface in an electrolyte solution are discussed. The potential distribution at the interface is analyzed in detail by solution of the Poisson equation in the absence of trapped charge at the interface, resulting in expressions for the space charge layer capacitance as a function of the band bending under depletion and accumulation conditions. The influence of the Helmholtz layer capacitance is incorporated in the analysis, while the influence of specific adsorption is discussed qualitatively. The semiconductor – electrolyte interface is characterized by electrically active surface states and recombination centers, which can also affect the potential distribution accross the interface. These processes are discussed in detail using a quantitative kinetic analysis, specifically aimed at the experimental methods used to determine the effects. Electrochemical impedance spectroscopy is shown to be sensitive to all processes that upon application of a modulated potential result in a modulated

current in the external circuit. Careful experiments as a function of the applied potential and modulation frequency give information on the energetics at the interface as well as processes involving surface states or recombination centers. Intensity-modulated photocurrent spectroscopy is very useful for the elucidation of minority carrier processes including recombination. Potential-modulated microwave reflectivity spectroscopy is a relatively new method specifically suited for the separation of free carrier processes and interface state processes. Examples are given for silicon surfaces in a variety of electrolyte solutions, illustrating the applicability of the techniques and the validity of the calculations.

## BIBLIOGRAPHY


1. W. Kern (ed.), *Handbook of Semiconductor Wafer Cleaning Technology: Science, Technology, and Applications*, Park Ridge, NJ: Noyes Publications, 1993.
2. C. Kittel, *Introduction to Solid State Physics*, 7th ed., New York: John Wiley & Sons, 1996.
3. S. M. Sze, *Physics of Semiconductor Devices*, 2nd ed., New York: John Wiley & Sons, 1981.
4. S. L. Chuang, *Physics of Optoelectronic Devices*, New York: John Wiley & Sons, 1995.
5. A. Many, Y. Goldstein, and N. B. Grover, *Semiconductor Surfaces*, Amsterdam: North-Holland Publishing Company, 1965.
6. J. B. Hudson, *Surface Science: An Introduction*, Boston: Butterworth-Heinemann, 1992.
7. W. Mönch, *Semiconductor Surfaces and Interfaces*, Berlin: Springer-Verlag, 1993.
8. A. J. Bard and L. R. Faulkner, *Electrochemical Methods: Fundamentals and Applications*, New York: John Wiley & Sons, 1980.
9. S. R. Morrison, *Electrochemistry at Semiconductor and Oxidized Metal Electrodes*, New York: Plenum Press, 1980.
10. Yu. V. Pleskov and Yu. Ya. Gurevich, *Semiconductor Photoelectrochemistry*, New York: Consultants Bureau, 1986.
11. H. O. Finklea (ed.), *Semiconductor Electrodes*, Amsterdam: Elsevier, 1988.
12. A. J. Bard, R. Parsons, and J. Jordan (eds.), *Standard Potentials in Aqueous Solutions*, Dekker: New York, 1985.
13. W. Schmickler, *Interfacial Electrochemistry*, Oxford University Press: Oxford, 1996.
14. J. R. Macdonald (ed.), *Impedance Spectroscopy*, New York: John Wiley & Sons, 1987.
15. W. M. Bullis, D. G. Seiler, and A. C. Diebold, *Semiconductor Characterization: Present Status and Future Needs*, Woodbury, (NY): American Institute of Physics Press, 1996.
16. (a): D. Vanmaekelbergh, Direct and surface state mediated electron transfer at semiconductor/electrolyte junctions—I. A comparison of steady-state results, *Electrochim. Acta*, **42** (7), 1121–1134, 1997.
    (b): D. Vanmaekelbergh, Direct and surface state mediated electron transfer at semiconductor/electrolyte junctions—II. A comparison of the interfacial admittance, *Electrochim. Acta*, **42** (7), 1135–1141, 1997.
17. (a): G. Oskam, P. M Hoffmann, J. C. Schmidt, and P. C. Searson, Energetics and kinetics of surface states at *n*-type silicon surfaces in aqueous fluoride solutions, *J. Phys. Chem.*, **100**, 1801–1806, 1996.
    (b): P. M. Hoffmann, G. Oskam, and P. C. Searson, Analysis of the impedance response due to surface states at the semiconductor/solution interface, *J. Appl. Phys.*, **83**, 4309–4323, 1998.
18. D. Vanmaekelbergh, A. R. de Wit, and F. Cardon, Recombination in semiconductor electrodes: investigation by the electrical and optoelectrical impedance method, *J. Appl. Phys.*, **73** (10), 5049–5057, 1993.
19. (a): G. Oskam, J. C. Schmidt, P. M. Hoffmann, and P. C. Searson, Electrical properties of *n*-type (111) Si in aqueous $K_4Fe(CN)_6$ solution: I. Interface states and recombination impedance, *J. Electrochem. Soc.*, **143** (8), 2531–2537, 1996.
    (b): G. Oskam, J. C. Schmidt, and P. C. Searson, Electrical properties of *n*-type (111) Si in aqueous $K_4Fe(CN)_6$ solution: II. Intensity Modulated Photocurrent Spectroscopy, *J. Electrochem. Soc.*, **143** (8), 2538–2543, 1996.
20. L. M. Peter, J. Li, R. Peat, H. J. Lewerenz, and J. Stumper, Frequency response analysis of intensity modulated photocurrents at semiconductor electrodes, *Electrochim. Acta*, **35** (10), 1657–1664, 1990.
21. (a): G. Schlichthörl and H. Tributsch, Microwave photoelectrochemistry, *Electrochim. Acta*, **37** (5), 919–931, 1992.
    (b): A. Natarajan, G. Oskam, and P. C. Searson, Characterization of silicon surfaces in HF solution using microwave reflectivity, *J. Appl. Phys.*, **83**, 2112–2120, 1998.
    (c): A. Natarajan, A. Nellore, and P. C. Searson, Theory of potential modulated microwave reflectivity at semiconductor surfaces, *J. Appl. Phys.*, **85**, 1631–1636, 1999.



GERKO OSKAM
PETER M. HOFFMANN
ARUN NATARAJAN
PETER C. SEARSON
John Hopkins University
Baltimore, MD